Cortical Microtubule Arrays Are Initiated from a Nonrandom Prepattern Driven by Atypical Microtubule Initiation[1][W][OA]

Jelmer J. Lindeboom*, Antonios Lioutas, Eva E. Deinum, Simon H. Tindemans, David W. Ehrhardt, Anne Mie C. Emons, Jan W. Vos, and Bela M. Mulder

Laboratory of Cell Biology, Wageningen University, 6708 PB Wageningen, The Netherlands (J.J.L., A.L., A.M.C.E., J.W.V., B.M.M.); Foundation for Fundamental Research on Matter, Institute for Atomic and Molecular Physics, 1098 XG Amsterdam, The Netherlands (E.E.D., S.H.T., A.M.C.E., B.M.M.); Department of Plant Biology, Carnegie Institution for Science, Stanford, California 94305 (D.W.E.); and Department of Biology, Stanford University, Stanford, California 94305 (D.W.E.)

The ordered arrangement of cortical microtubules in growing plant cells is essential for anisotropic cell expansion and, hence, for plant morphogenesis. These arrays are dismantled when the microtubule cytoskeleton is rearranged during mitosis and reassembled following completion of cytokinesis. The reassembly of the cortical array has often been considered as initiating from a state of randomness, from which order arises at least partly through self-organizing mechanisms. However, some studies have shown evidence for ordering at early stages of array assembly. To investigate how cortical arrays are initiated in higher plant cells, we performed live-cell imaging studies of cortical array assembly in tobacco (*Nicotiana tabacum*) Bright Yellow-2 cells after cytokinesis and drug-induced disassembly. We found that cortical arrays in both cases did not initiate randomly but with a significant overrepresentation of microtubules at diagonal angles with respect to the cell axis, which coincides with the predominant orientation of the microtubules before their disappearance from the cell cortex in preprophase. In Arabidopsis (*Arabidopsis thaliana*) root cells, recovery from drug-induced disassembly was also nonrandom and correlated with the organization of the previous array, although no diagonal bias was observed in these cells. Surprisingly, during initiation, only about one-half of the new microtubules were nucleated from locations marked by green fluorescent protein-γ-tubulin complex protein2-tagged γ-nucleation complexes (γ-tubulin ring complex), therefore indicating that a large proportion of early polymers was initiated by a noncanonical mechanism not involving γ-tubulin ring complex. Simulation studies indicate that the high rate of noncanonical initiation of new microtubules has the potential to accelerate the rate of array repopulation.

Higher plant cells feature ordered arrays of microtubules at the cell cortex (Ledbetter and Porter, 1963) that are essential for cell and tissue morphogenesis, as revealed by disruption of cortical arrays by drugs that cause microtubule depolymerization (Green, 1962) or stabilization (Weerdenburg and Seagull, 1988) and by loss-of-function mutations in a wide variety of microtubule-associated proteins (Baskin, 2001; Whittington et al., 2001; Buschmann and Lloyd, 2008; Lucas et al., 2011). The structure of these arrays is thought to control the pattern of cell growth primarily by its role in the deposition of cellulose microfibrils, the load-bearing component of the cell wall (Somerville, 2006). Functional relations between cortical microtubules and cellulose microfibrils have been proposed since the early sixties, even before cortical microtubules had been visualized (Green, 1962). Recent live-cell imaging studies have confirmed that cortical microtubules indeed guide the movement of cellulose synthase complexes that produce cellulose microfibrils (Paredez et al., 2006) and have shown further that microtubules position the insertion of most cellulose synthase complexes into the plasma membrane (Gutierrez et al., 2009). These activities of ordered cortical microtubules are proposed to facilitate the organization of cell wall structure, creating material properties that underlie cell growth anisotropy.

While organization of the interphase cortical array appears to be essential for cell morphogenesis, this organization is disrupted during the cell cycle as

[1] This work was supported by the European Union FP6–2004–NEST–C1 project 028974 (CASPIC to J.J.L., A.M.C.E., and B.M.M.), the Netherlands Genomics Initiative/Nederlandse Organisatie voor Wetenschappelijk Onderzoek (NWO) research program of the Netherlands Consortium for Systems Biology (to E.E.D.), the "Stichting voor Fundamenteel Onderzoek der Materie" (to B.M.M.), which is financially supported by the NWO, the NWO Computational Life Science program (grant no. CLS 635.100.003 to S.H.T.), an NWO VENI grant (no. 863.02.009 to J.W.V.), the NWO/Netherlands Institute for Space Research (grant no. GO–MG/01 to J.W.V.), the National Science Foundation (grant no. 0524334 to D.W.E.), and by the European Union NEST network (CASPIC grant no. 28974 to D.W.E.).

* Corresponding author; e-mail jelmer.lindeboom@wur.nl.

The author responsible for distribution of materials integral to the findings presented in this article in accordance with the policy described in the Instructions for Authors (www.plantphysiol.org) is: Jelmer J. Lindeboom (jelmer.lindeboom@wur.nl).

[W] The online version of this article contains Web-only data.

[OA] Open Access articles can be viewed online without a subscription.

www.plantphysiol.org/cgi/doi/10.1104/pp.112.204057

microtubules are rearranged to create the preprophase band, spindle, and phragmoplast during mitosis and cytokinesis (for review, see Wasteneys, 2002). Upon completion of cytokinesis, an organized interphase cortical array is regenerated, but the pathway for this reassembly is not well understood.

The plant interphase microtubule array is organized and maintained without centrosomes as organizing centers (for review, see Wasteneys, 2002; Bartolini and Gundersen, 2006; Ehrhardt and Shaw, 2006), and microtubule self-organization is proposed to play an important role in cortical microtubule array ordering (Dixit and Cyr, 2004). In electron micrographs, microtubules have been observed to be closely associated with the plasma membrane (Hardham and Gunning, 1978), and live-cell imaging provides evidence for attachment of microtubules to the cell cortex (Shaw et al., 2003; Vos et al., 2004). The close association to the plasma membrane restricts the cortical microtubules to a quasi two-dimensional plane where they interact through polymerization-driven collisions (Shaw et al., 2003; Dixit and Cyr, 2004). Microtubule encounters at shallow angles (<40°) have a high probability of leading to bundling, while microtubule encounters at steeper angles most likely result in induced catastrophes or microtubule crossovers (Dixit and Cyr, 2004). Several computational modeling studies have since shown that these types of interactions between surface-bound dynamical microtubules can indeed explain spontaneous coalignment of microtubules (Allard et al., 2010; Eren et al., 2010; Hawkins et al., 2010; Tindemans et al., 2010).

The question of how the orientation of the cortical array is established with respect to the cell axis is less well understood. One possibility is that microtubules are selectively destabilized with respect to cellular coordinates (Ehrhardt and Shaw, 2006). Indeed, recent results from biological observations and modeling suggest that catastrophic collisions induced at the edges between cell faces or heighted catastrophe rates in cell caps could be sufficient to selectively favor microtubules in certain orientation and hence determine the final orientation of the array (Allard et al., 2010; Eren et al., 2010; Ambrose et al., 2011; Dhonukshe et al., 2012).

To date, all models of cortical array assembly assume random initial conditions. However, experimental work by Wasteneys and Williamson (1989a, 1989b) in *Nitella tasmanica* showed that, during array reassembly after drug-induced disruption, microtubules were initially transverse. This was followed by a less ordered phase and later by the acquisition of the final transverse order. A nonrandom initial ordering was also observed in tobacco (*Nicotiana tabacum*) Bright Yellow-2 (BY-2) cells by Kumagai et al. (2001), who concluded that the process of transverse array establishment starts with longitudinal order but did not provide quantitative data for the process of array assembly. The initial conditions for the cortical microtubule array formation are important to consider, as they may strongly influence the speed at which order is established and could even prevent it from being established over a biologically relevant time scale.

In this study, we used live-cell imaging to follow and record the whole transition from the cortical microtubule-free state to the final transverse array and used digital tracking algorithms to quantify the microtubule order. Nucleation stands out as a central process to characterize during array initiation. Lacking a central body to organize microtubule nucleations, the higher plant cell has dispersed nucleation complexes (Wasteneys and Williamson, 1989a, 1989b; Chan et al., 2003; Shaw et al., 2003; Murata et al., 2005; Pastuglia et al., 2006; Nakamura et al., 2010). Therefore, we performed high time resolution observations to quantify nucleation complex recruitment, nucleation rates, and microtubule nucleation angles. We found evidence for a highly nonrandom initial ordering state that features diagonal microtubule orientation and an atypical microtubule initiation mechanism. Simulation analysis indicates that these atypical nucleations have the potential to accelerate the recovery of cortical array density.

RESULTS

After Cytokinesis, Microtubules in BY-2 Cells Reappear with a Transient Diagonal Order

To investigate array initiation, we used tobacco BY-2 suspension cells expressing GFP fused to tobacco α-tubulin (GFP-TUA). These cells feature highly ordered arrays oriented transversely to the axis of growth, have a relatively high mitotic index, and are ideal for drug treatment in flow cell experiments. Furthermore, the potential crosstalk with neighbors is limited because BY-2 cells generally grow in cell files that break up into individual cells (Chan et al., 2011; Crowell et al., 2011; Fujita et al., 2011).

Using point-scanning confocal microscopy, we acquired images from the plane of the cell cortex every 3 to 5 min and measured microtubule length density and ordering after cytokinesis. The first visible microtubules appeared in the cortex after the phragmoplast reached the optical plane of the cell cortex (Fig. 1A; Supplemental Fig. S1; Supplemental Movie S1) and within approximately 45 min the length density, defined as microtubule length per square micrometer, leveled at around 0.5 $\mu m/\mu m^2$ (μm^{-1}, mean of six cells; Fig. 1B). With the increase in length density, the microtubules also became increasingly bundled, as indicated by increases in the fluorescence intensities of individual microtubule structures. As our focus was on microtubule orientation, we gave bundles the same weight as individual microtubules.

The angles of microtubules with respect to the cell elongation axis were measured and visualized in a contour plot (Fig. 1C). Time is presented along the x axis, and the angular distribution over the interval from 0° to 180° along the y axis (20 bins). The color range represents the fraction of the total microtubule length, so that orientation patterns at both low and high microtubule densities can be compared. Surprisingly, the majority of the microtubule length was diagonally oriented at 45° and 135° angles to the elongation axis in the

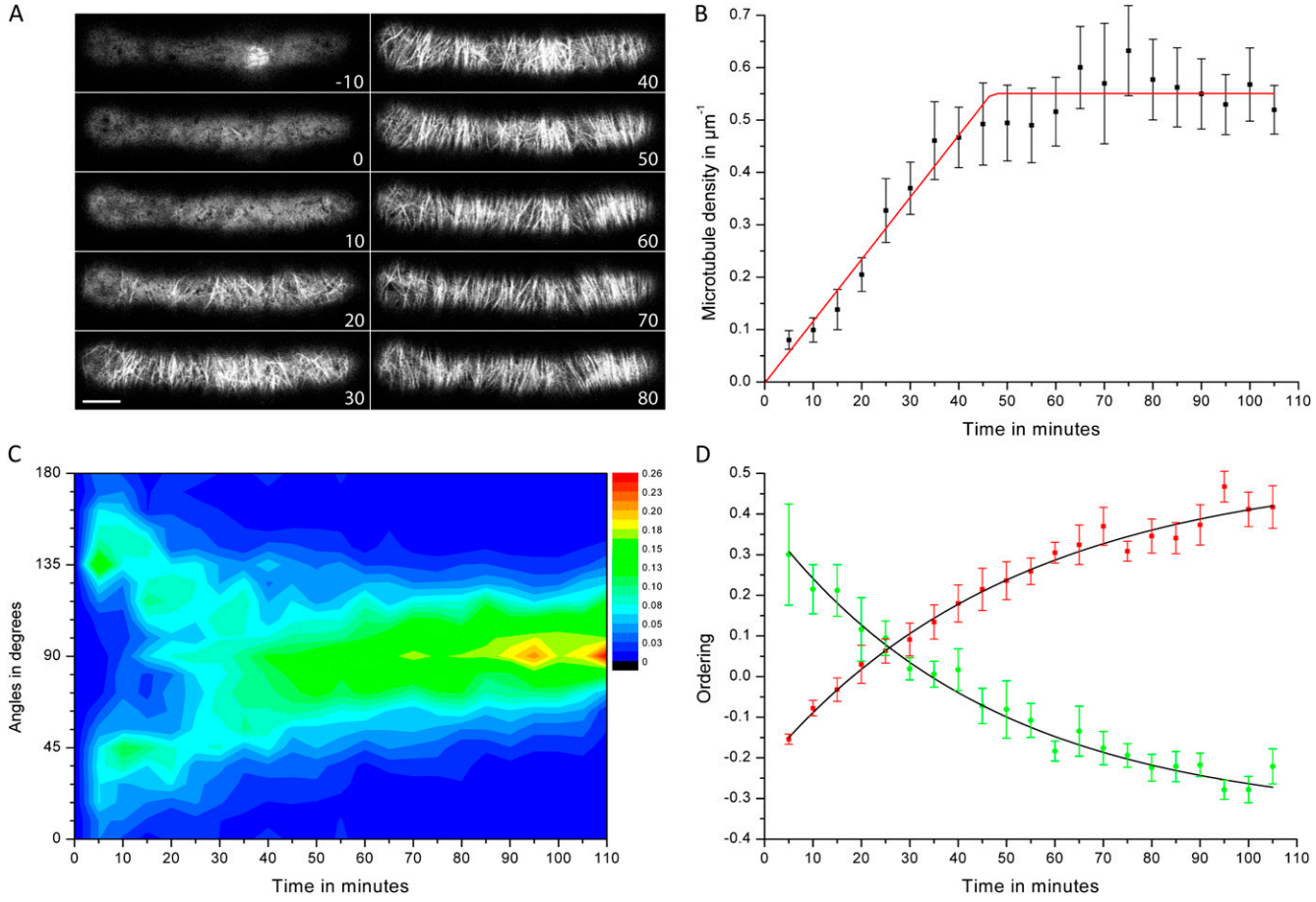

Figure 1. Return of cortical microtubules after cell division in BY-2 cells. A, Cortical microtubules in two daughter cells after cytokinesis. The first frame (–10 min) shows the late phragmoplast in the cortex. Bar = 10 μm. B, Microtubule length density increase over time after cytokinesis (mean of six cells). The mean density plateaus at approximately 0.54 μm^{-1} and is reached after approximately 46 min, based on linear curve fitting of the individual data points of six cells (red line). Bars represent SE. C, Angular distribution over time presented as the fraction of the total microtubule length at each measurement (mean of six cells). The first microtubules are ordered along the diagonal cell axes of 45° and 135°. D, *D* (green circles and error bars) and *T* (red squares and error bars) microtubule order parameters after cell division (mean of six cells ± SE) and the exponential curve fittings (black lines, based on all individual data points). At approximately 25 min after t_0 (last measurement before microtubules became visible), the transverse microtubule ordering became dominant over the diagonal microtubule order.

early stages of array reformation, forming two clear peaks in the angular frequency histogram.

To quantify the transition from the diagonal to the transverse cortical microtubule order, the angular distribution data were filtered to produce the weighted diagonal order parameter *D* and the weighted transverse order parameter *T* (see Supplemental Materials and Methods S1). From the means of the *D* and *T* order parameters over time, we infer that the diagonal ordering was dominant for the first approximately 25 min, after which it was replaced by transverse ordering (Fig. 1D).

Transient Diagonal Ordering during Recovery from Oryzalin Treatment in BY-2 Cells

To establish if the mechanism of transverse microtubule ordering via a transient diagonal phase is generic or cell cycle dependent, we immobilized BY-2 cells expressing GFP-TUA in flow cells and treated them for 1 h with 20 μM oryzalin to reversibly depolymerize the cortical microtubule array (Morejohn et al., 1987; Fig. 2A; Supplemental Movie S2). This concentration and duration of oryzalin treatment was sufficient to eliminate all detectible GFP-TUA-labeled microtubules. Both the microtubule length density increase and the development of ordering after oryzalin washout were similar as observed after cell division (Fig. 2B). The average plateau density was reached approximately 25 min after appearance of the first cortical microtubules, which is approximately 45 min after the start of the oryzalin washout (mean of eight cells). The first microtubules reappeared at diagonal angles to the elongation axis (45° and 135°; Fig. 2C). On average, the transient diagonal ordering was replaced by the final transverse ordering after approximately 40 min (Fig. 2D). Thus, it

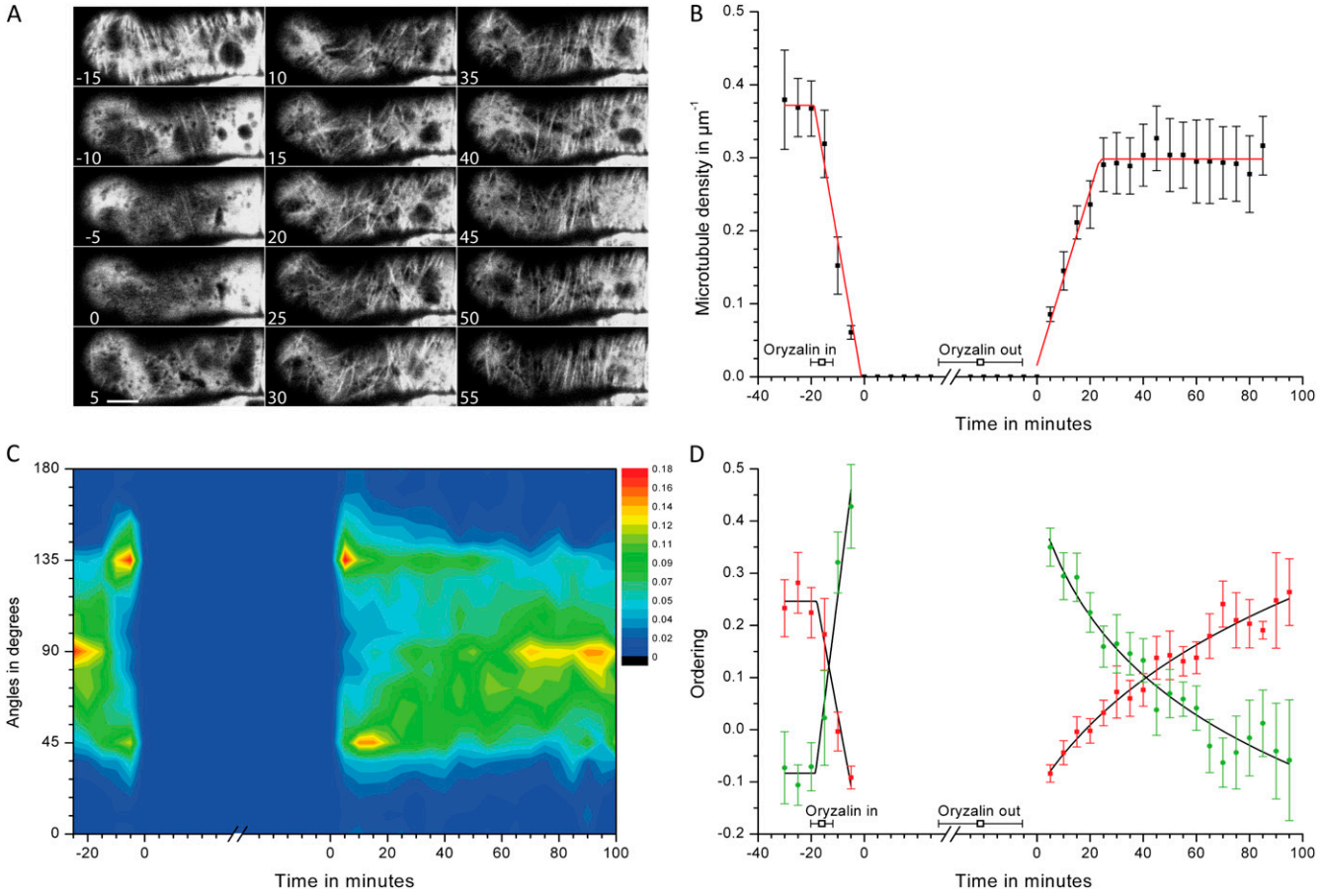

Figure 2. Treatment of GFP-TUA-expressing BY-2 cells with oryzalin. A, Cortical microtubules before, during, and after incubation with 20 μM oryzalin in a flow cell. Oryzalin was added at –15 minutes and washed out again after 60 min by continuous washing with BY-2 culture medium. Bar = 10 μm. B, Microtubule length density in oryzalin treatment over time (mean of eight cells). The individual cells of the oryzalin treatments were aligned relative to the observation point at which no microtubules were visible after oryzalin addition and to the point at which no microtubules were yet visible after oryzalin washout. Both are referred to as T_0 in the text and figures. Imaging was continued during depolymerization, and all images were checked for microtubules. At -16 ± 2 min (mean $\pm$ SE), 20 μM oryzalin was added and washed out again after 60 min. About 21 $\pm$ 6 min (mean $\pm$ SE) after oryzalin washout, the first cortical microtubules started to reappear. C, Averaged angular distribution over time presented as the fraction of the total microtubule length at each measurement (mean of eight cells). Just after addition of oryzalin at the start of recovery after washout, diagonal microtubules are dominant. D, *D* (green error bars) and *T* (red error bars) cortical microtubule ordering parameters over time in oryzalin treatment experiments (means of eight cells $\pm$ SE). Less than 2 min after oryzalin addition, *D* (green circles) became dominant over *T* (red squares) based on the intercept of the linear curve fittings of the individual data points (black lines). After oryzalin washout, diagonal ordering became apparent and remained dominant for approximately 36 min, based on the intercept of the exponential curve fittings (black lines), followed by dominance of the transverse microtubule array.

appears that both the pattern and kinetics of assembly and ordering are similar whether the array is disassembled by native mechanisms during the cell cycle or by drug treatment.

Diagonal Ordering Also Occurs during Array Disassembly in BY-2 Cells

Interestingly, a diagonal bias for microtubule orientation was also observed during late stages of array disassembly as cells exit interphase and form preprophase bands (observations from five cells; Supplemental Fig. S2). Likewise, the same bias was observed in late stages of microtubule depolymerization caused by oryzalin application (Fig. 2, C and D). The microtubule length density started to decrease less than a minute after drug application and reached zero microtubules after approximately 16 min. Within 2 min after oryzalin addition, a diagonal microtubule order took over the dominant transverse order and lasted until the last microtubules were depolymerized (Fig. 2D). Thus, diagonal biasing of microtubule orientation appears to be a feature both of the last stages of array disassembly and the first stages of array reassembly, irrespective of whether arrays are taken apart by cellular mechanisms or by drug treatment.

Microtubule Nucleation Has a Diagonal Bias during Array Initiation in BY-2 Cells

A bias in microtubule orientation might occur because microtubules are preferentially created in specific orientations, because they are selectively destabilized, or if they are reoriented once initiated. To assess the origin of the diagonal microtubule ordering, we made movies at high time resolution (2-s intervals) of BY-2 cells expressing GFP-TUA cytokinesis and oryzalin washout (Supplemental Movie S3). We observed that in the first 30 min, the majority of new microtubules were nucleated at the cell cortex at locations free of other detectable microtubules. The majority of nucleations during this period were free nucleations (274 out of 352, 77%, in six cells after cytokinesis, and 73 out of 117, 62%, in five cells after oryzalin washout). These observations are in contrast with those of interphase nucleation, where microtubule-associated microtubule nucleations have been observed to comprise more than 99% of nucleations in wild-type Arabidopsis (*Arabidopsis thaliana*) cells (Murata et al., 2005; Nakamura et al., 2010; Kirik et al., 2012). We measured the angles of these free nucleations with respect to the cell axis after both cytokinesis (Fig. 3A) and oryzalin washout (Fig. 3B). We did not analyze microtubule nucleations in the same orientation as the microtubule they nucleated on, as they do not give rise to new microtubule orientations. A Bayesian statistical analysis of these data (see "Materials and Methods") revealed a significant bias for nucleations to occur along the diagonal directions both after cytokinesis and oryzalin washout.

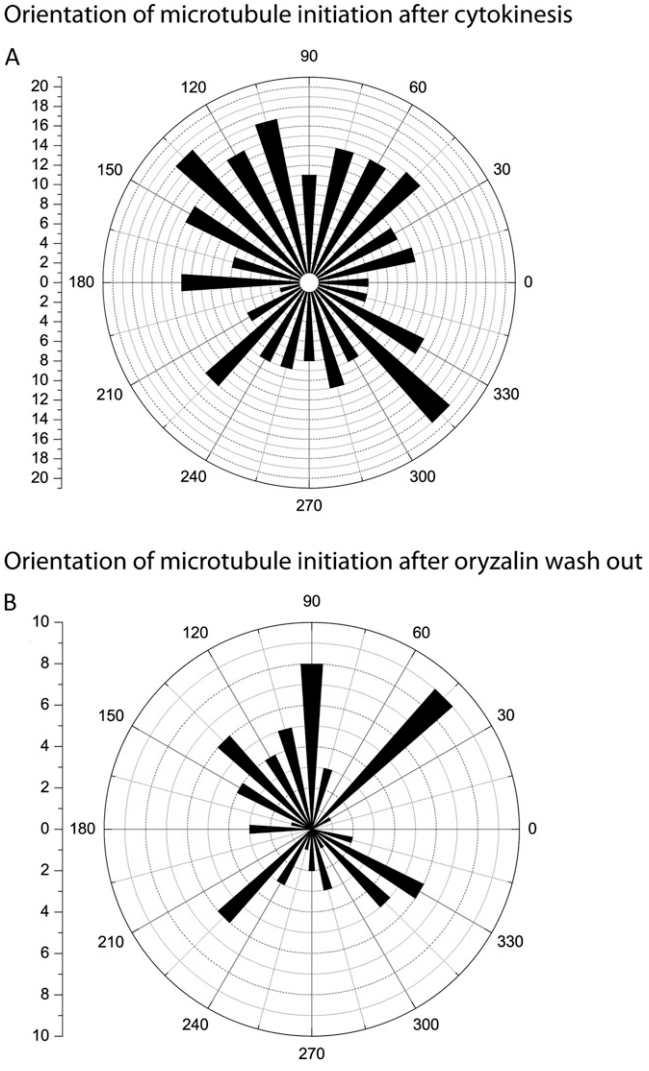

Figure 3. Free nucleations after cytokinesis and oryzalin washout. A and B, Polar histogram nucleation angles within the 30-min period after the first cortical microtubules appear after cytokinesis in tobacco BY-2 cells (274 nucleations, six cells; A) and oryzalin washout (117 nucleations in five cells; B). Angles in degrees; histogram scale is in number of observations.

In Arabidopsis Root Cells, a Large Fraction of Nucleations during Array Initiation Are Free of Labeled γ-Tubulin Complexes

We found it remarkable that the nucleation bias had the same orientation as the cortical microtubule order just before disappearance. This suggested that a "memory" of the previous array organization might be maintained at the cell cortex. We could imagine three alternative models. First, nucleation complexes recruited to the previous array might persist at the cell cortex, retaining orientational information. Second, there might be other orientational information at the cell cortex that acts to orient newly recruited nucleation complexes as they initiate the next array. Finally, a subset of the previous array might be resistant to disassembly either by native mechanisms or by drugs, and they may be either small enough to evade detection by GFP-TUA5 labeling (or that the specific isoform of α-tubulin we labeled is not or less incorporated into these structures). These disassembly-resistant remnants might act as orientated seeds for initiating new polymerization during array reassembly.

To distinguish among these hypotheses, we assayed the localization and dynamic behavior of γ-tubulin complexes and their relationship to new nucleations using Arabidopsis plants expressing both a γ-tubulin complex marker (γ-tubulin complex protein2 [GCP2]-triple GFP; Nakamura et al., 2010) and a compatible tubulin marker (mCherry-TUA5; Gutierrez et al., 2009; Supplemental Movie S4). To facilitate our analysis, we used a 1-h treatment of 1 μM oryzalin to dissemble existing cortical arrays in Arabidopsis root epidermal cells. After drug washout, we acquired images of the cell cortex at high time resolution (2-s intervals). We observed no evidence for persistent GFP-labeled nucleation complexes at the cell cortex, thus refuting the first hypothesis: that nucleation complexes recruited to the previous array might persist at the cell cortex to initiate the new array.

We then scored all observed nucleation events in the field of view, asking if GCP2-3xGFP was present at the position of microtubule nucleation. As labeled complexes

are present and motile in the streaming cytosol (Nakamura et al., 2010), we required that punctae GFP signal be present at the position of nucleation for at least two consecutive image frames to be scored positively. In control cells that were not pretreated with oryzalin, we found that 68 out of 70 nucleations (97%) colocalized with the GCP2-3xGFP label (Fig. 4A; Supplemental Movie S5; data acquired from six cells on six plants), a frequency in good agreement with the approximately 98% found by Nakamura et al. (2010) in hypocotyl cells. By contrast, in oryzalin-treated cells, only a little over one-half of the observed nucleations (45 out of 81; 56%) colocalized with the GCP2-3xGFP label in the first 20 min after the start of oryzalin washout, a dramatically lower proportion ($P < 0.0001$, one-tailed binomial test, eight cells). Thus, while only approximately 3% of nucleations was not observed to be accompanied by GCP2-3xGCP in mature arrays, this frequency raised to approximately 44% during early stages of array assembly (Fig. 4B). The lack of detectable γ-tubulin ring complex (γ-TuRC) label at nearly one-half of the early nucleations argues strongly against the second hypothesis for diagonal nucleation orientation: that orientational information at the cell cortex directs the orientation of new nucleation complexes recruited to the cell cortex during early array assembly. We also found no evidence for involvement of two candidates for such orientational information, the cortical actin cytoskeleton and cellulose microfibrils, by disruption experiments with latrunculin B (Supplemental Fig. S3) or isoxaben (Supplemental Fig. S4), respectively.

On the other hand, the marked reduction in GCP2-3xGFP colocalization was consistent with the third hypothesis: that a large and significant proportion of nucleations during early array recovery arises from seeds not associated with γ-tubulin complexes. We term these nucleation events noncanonical nucleations because they lack association with detectible γ-TuRCs as determined by GCP2-3xGFP labeling, an essential subunit of the core γ-TuRC.

In the Arabidopsis root epidermal cells, we also determined the orientation the orientation of the cortical microtubule array during oryzalin treatment and the recovery from oryzalin washout. We found that in these cells, the orientational bias of the initial array after oryzalin washout was the same as the bias that we found during the depolymerization (Fig. 4, C and D; Supplemental Fig. S5; Supplemental Movie S6). This was the case not only for transversely oriented cortical microtubule arrays, but also for oblique and longitudinal arrays (Fig. 4, C and D; Supplemental Fig. S5; Supplemental Movie S6).

Simulations

We performed mechanistic simulations to ask if the observed prevalence of diagonal microtubule nucleation was sufficient to explain the degree of observed diagonal ordering during the initial stages of array assembly and to ask what affect these noncanonical nucleations might have on the evolution of array density and ordering. In the simulations, cortical microtubules interact on a cylindrical cell-shaped surface of dimensions similar to that of the tobacco BY-2 cells used in our in vivo experiments (Fig. 5A; Tindemans et al., 2010; Deinum et al., 2011). To test for the influence of the noncanonical nucleation events, these nucleations were treated as a separate class; their density and orientations were chosen to match the distributions determined from the live-cell experiments as described above in BY-2 cells. At the start of the simulations, we add a finite pool of microtubule fragments with the density of 0.1 μm^{-2} and an activation rate of 0.003 s^{-1} (see "Materials and Methods" for further details on the simulation technique and the parameters employed). In simulations that include all nucleation events, the length density initially rises steeply, reaching approximately 80% of the final density in just 10 min, then transiently leveling off (Fig. 5B and illustrated in Fig. 4A at 15 min). By contrast, in simulations without the noncanonical nucleation class, the length density rises more gradually and steadily, reaching 80% of the final density only after about 40 min (Fig. 5B). Thus, the noncanonical nucleations appear to have the potential to significantly accelerate the recovery of array density during array reassembly.

When simulations were run without the noncanonical nucleation class, there was no initial bias of the angular distribution (Fig. 5C). As expected, when these nucleations were added to the simulation, a clear initial bias at 45° and 135° is created (Fig. 5D), markedly similar to our experimental observations (Fig. 1C). The D and T order parameters, as a function of time for the simulations with the noncanonical nucleation class (Fig. 5E), both qualitatively and quantitatively match the values we found experimentally (Fig. 5D). Thus, the inclusion of the diagonally biased nucleation events observed in living cells has the potential to explain both the initial diagonal ordering and the observed evolution of array ordering in these cells. While noncanonical nucleations had the effect of lowering the initial transverse ordering state of the simulated arrays, the difference is not significant and the order parameters level off to the same value (Fig. 5F), indicating that biased noncanonical nucleations did not present a barrier to achieving proper array ordering.

DISCUSSION

The transverse arrangement of the cortical microtubule array is essential for anisotropic growth, yet little was known about how it arises from a disassembled state, the situation that recurs after each cell division during the life of the cell. The currently accepted self-organization models for transverse cortical microtubule array establishment, based on microtubule interactions (Allard et al., 2010; Eren et al., 2010; Hawkins et al.,

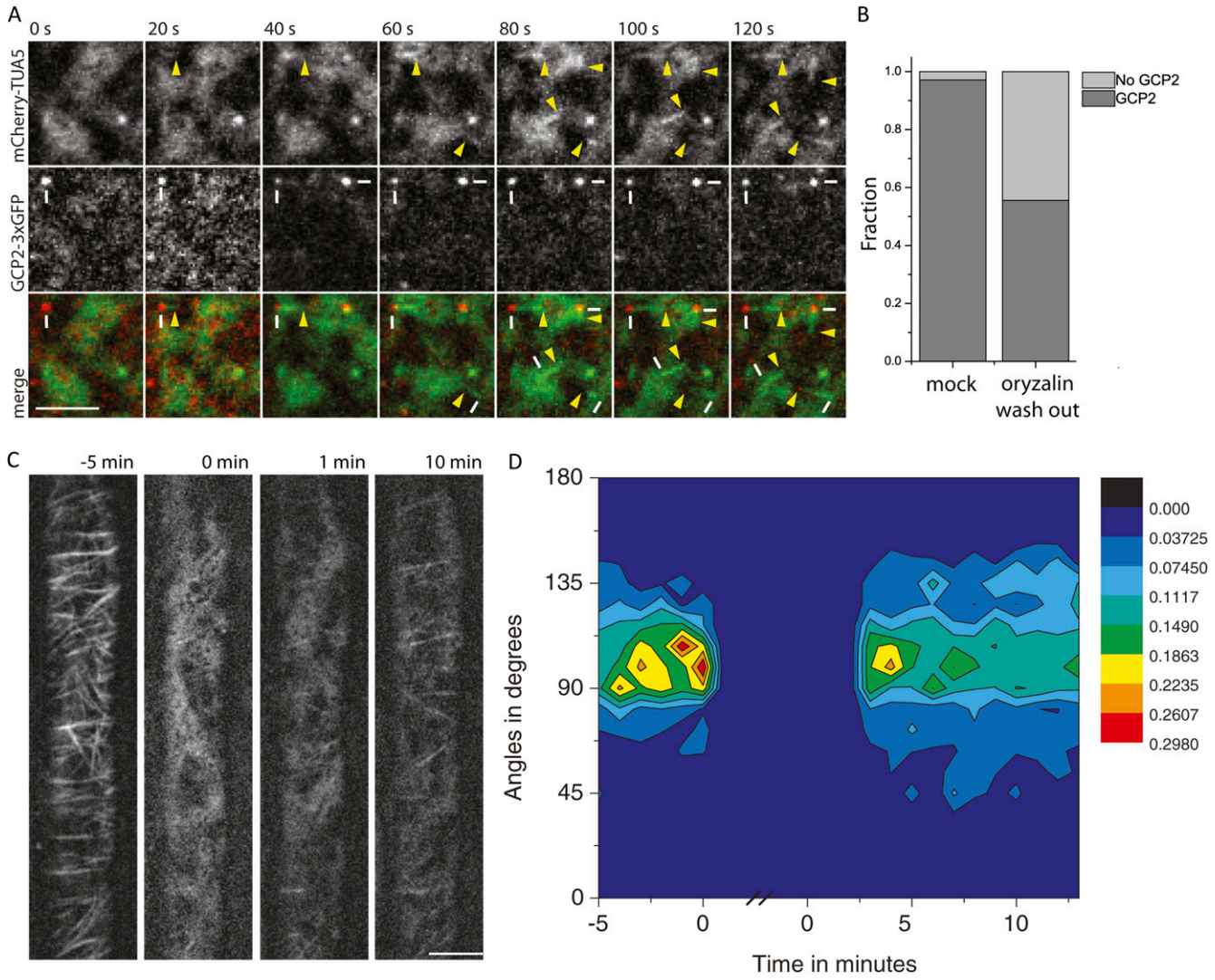

Figure 4. Oryzalin treatment in Arabidopsis root epidermal cells. A, Example of free nucleations after oryzalin washout in Arabidopsis root epidermal cells. Dashes indicate microtubule minus ends; arrowheads indicate microtubule plus ends. Two out of four nucleations in this image sequence show a GCP2-3xGFP signal. Bar = 3 μm. B, Bar graph of the fraction of nucleations where GCP2-3xGFP signal was detected or not. Results are shown for untreated Arabidopsis root cells (70 nucleations) and after oryzalin washout (81 nucleations). C, Cortical microtubules before, during, and after incubation with 1 μM oryzalin in a flow cell. Oryzalin was added at −5 min and washed out again after 60 min by continuous washing. Bar = 5 μm. D, Angular distribution over time presented as the fraction of the total microtubule length at each measurement. The orientational bias of the cortical microtubules after breakdown by oryzalin closely resembles the orientational bias before the oryzalin treatment.

2010; Tindemans et al., 2010), assume that new microtubules appear with random initial orientations. We found that the first microtubules in new arrays of tobacco BY-2 cells were in fact not randomly oriented but showed significant ordering at orientations of both 45° and 135°. This was true both for array assembly during the cell cycle as well as reassembly of arrays after oryzalin washout. Organization in these arrays did not evolve by gradual ordering from a disorganized, random state but by a transition from one ordered state to another.

Exploration of the cause for the nonrandom initiation of array establishment revealed that there was a significant bias in the orientation of early microtubule nucleations, sharing the same 45° and 135° bias relative to the cell axis that was observed for array ordering. Results from simulation studies incorporating these oriented nucleations matched experimental observations very closely, indicating that this population of directionally biased nucleations is sufficient to explain the fast-forming initial diagonal ordering state of new arrays, and together with self-ordering based on microtubule interactions, is sufficient to explain the transition from this transiently ordered array into the final transverse array.

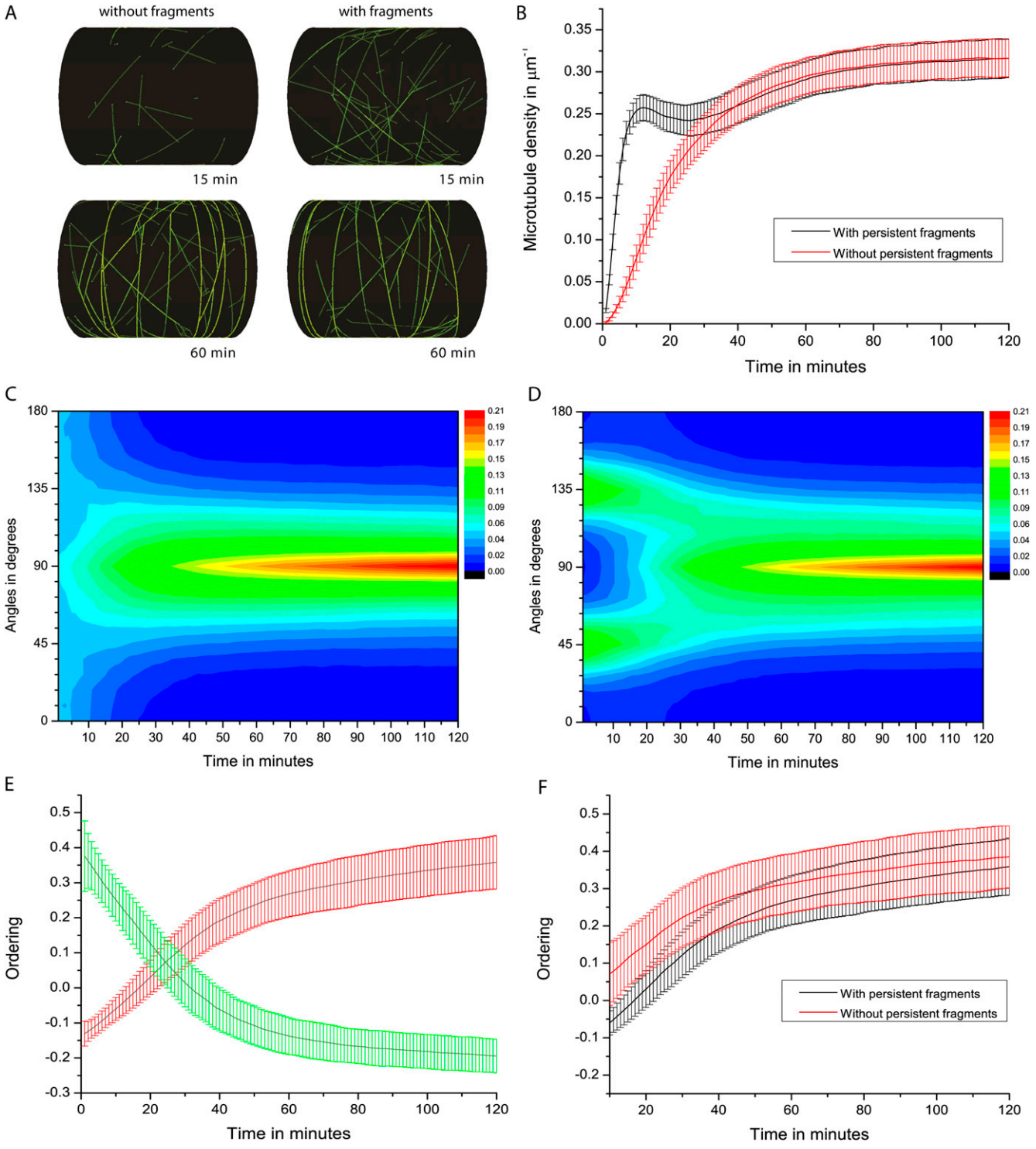

Figure 5. Results of the simulations. A, Snapshots of representative microtubule configurations at 15 and 60 min after the start of the simulation both with (right) and without (left) persistent fragments. B, The time evolution of the average (optical) density of microtubules for the simulations with and without persistent fragments. Error bars = 1 SD. C and D, Averaged angular distribution over time presented as the fraction of the total (optical) microtubule length from simulations without (C) and with (D) persistent microtubule fragments. E, The time evolution of the average *D* (green error bars) and *T* (red error bars) cortical microtubule ordering parameters. The gray lines represent the average value. Error bars = 1 SD. F, Comparison of the evolution of the transverse order parameter *T* in the simulations, with and without persistent microtubule fragments. All simulation results are combined for 500 individual simulations.

Analysis of oryzalin treatment in Arabidopsis root epidermal cells showed that also in these cells, the initial bias of microtubule orientation correlates with the last orientation before disassembly. This was true for not only the transverse cortical microtubule array but also for oblique and longitudinal orientation, which strongly suggests that the bias depends on elements of the microtubule cytoskeleton before depolymerization.

We considered several alternative ideas for the mechanism of nucleation orientation. In interphase cells, the majority of nucleations at the cell cortex occurs from the sides of existing microtubules with a major peak at about 40° (Murata et al., 2005) and a secondary peak at 0° (i.e. parallel to the parent polymer; Chan et al., 2009; Nakamura et al., 2010; Kirik et al., 2012). Thus, in the interphase arrays studied to date, existing microtubules largely determine the orientation of new microtubule nucleation. The vast majority of the nucleation events in the cortex of Arabidopsis interphase cells have been observed to be marked by tagged components of the γ-TuRC complex (>98%; Nakamura et al., 2010; Kirik et al., 2012). However, at the start of array assembly, there are no obvious existing microtubules (this study; Wasteneys and Williamson, 1989a, 1989b) to recruit and position nucleation complexes (Nakamura et al., 2010); therefore, it was necessary to consider other mechanisms for nucleation orientation. One possibility was that oriented γ-TuRC complexes are simply retained at the cell membrane from the previous cortical array, an idea that was directly contradicted by our observations in Arabidopsis root cells. A second possibility was that newly recruited γ-TuRCs are positioned by cryptic orientational information at the cortex. Surprisingly, however, we found that labeled γ-TuRC complexes failed to be detected at approximately 44% of the nucleation events observed during array initialization compared with approximately 3% at steady-state microtubule density. This result both effectively eliminated a mechanism based solely on oriented γ-TuRCs and revealed that many early nucleations apparently arise from noncanonical nucleation sites that lack a γ-TuRC. The GCP2 protein is a core component of the γ-TuRC complex and localizes to both mitotic and interphase microtubule arrays. The possibility that less of the GCP2 protein, which we use as the γ-TuRC complex marker, is incorporated in the γ-TuRC complexes therefore appears to be small, ruling out a bias due to insufficient labeling.

We do not know the molecular identity of the microtubule cytoskeleton elements that provide the seeding for the initial bias in microtubule initiation and ordering. While most microtubules are nucleated by γ-TuRCs (Teixidó-Travesa et al., 2012), nucleation has also been found to be facilitated by several microtubule plus end-binding proteins (Rogers et al., 2008; Rusan and Rogers, 2009), transforming acidic coiled-coil family proteins, and RanGTP-activated factors (Gruss and Vernos, 2004; Clarke and Zhang, 2008). It is not clear whether all these factor act as true nucleators or if they might stabilize short microtubule fragments that could act to restart polymer growth (Teixidó-Travesa et al., 2012). When we washed out oryzalin in Arabidopsis epidermal root cells after 30 min, short but still-visible fragments of microtubules started to reinitiate growth (Supplemental Movie S7). The noncanonical microtubule initiations we describe in this article are most likely not derived from γ-TuRC complexes because of the absence of GCP2-3xGPF marker at the cell cortex during the disassembly phase, suggesting that another factor may serve as the nucleator or that initiations may arise from stabilized short fragments of microtubules.

We therefore speculate that short fragments of microtubules may act as nucleators during early cortical array recovery. This would provide a mechanism by which the orientation of new initiations is tied to that of the previous array, in the absence of a microtubule scaffold that positions and orients nucleation complexes. Previous studies by Wasteneys and Williamson (1989b) in *N. tasmanica* are also consistent with this possibility. These investigators observed that while *N. tasmanica* microtubules returned in their original transverse orientation during recovery from oryzalin, orientation was random after longer, and presumably more complete, oryzalin treatment (Wasteneys and Williamson, 1989a, 1989b). In our studies, incomplete drug action cannot explain observations of array reassembly following cytokinesis, since there was no drug treatment in these cells and the extremely similar mode and kinetics of array reassembly we observed between these cells and those recovering from oryzalin treatment suggest that a similar mechanism is responsible in both situations.

It is as yet unclear how such sort pieces of microtubules persist at the cell cortex during drug treatments for over an hour and even longer during cytokinesis. We did observe that the rate of disassembly slows down over time. It is quite possible that microtubule disassembly is in part dependent on how much the microtubule is physically loaded with microtubule-associated proteins. Indeed, disassembly of microtubules could elevate the cytosolic concentration of microtubule-associated proteins by decreasing the microtubule binding surface. An increased concentration of free microtubule-associated proteins in turn could drive association with any polymer remaining, potentially acting to stabilize short microtubule fragments.

A number of questions remain. First, microtubule seeds from the previous cell cycle were not readily detected by imaging of GFP-TUA. However, this might be easily explained if the seeds are small enough to contain only a few labeled subunits (only a fraction of α-subunits in the cell are tagged), a degree of labeling that may well lie below the high background of unpolymerized subunits in the cytosol. It is also formally possible that the seeds may have a composition that does not include the labeled tubulin isoform used

for imaging. Such small fragments would be difficult to detect in electron micrographs because of their small size and their relatively low estimated density (0.1 μm^2).

A second puzzle is why the presumed source of the oriented seeds, the last cohort of microtubules at the end of array disassembly, has a diagonal bias to the cell axis in the BY-2 cells. One possibility is that the bias arises from the normal formation of the newest microtubules by branching nucleation at about 40° to their mother polymers (Wasteneys and Williamson, 1989a, 1989b; Murata et al., 2005; Chan et al., 2009; Nakamura et al., 2010). In a transversely oriented array, these nucleations would lie approximately at 45° and 135° to the cell axis and would have a high likelihood of interacting with the dominant population of transverse microtubules. These interactions can lead to incorporation into bundles by treadmilling motility (Shaw et al., 2003; Dixit and Cyr, 2004) or catastrophe (Dixit and Cyr, 2004), both of which would tend to diminish the population of diagonally oriented polymers. However, as the microtubule array is broken down and microtubule density drops, encounters would be predicted to be less frequent; therefore, the likelihood of aligning or eliminating branching microtubules will be reduced.

It is also not clear why there is a transient diagonally ordered phase during disassembly in BY-2 cells and not in our experiments in Arabidopsis root epidermal cells. The disassembly occurred approximately 5 times faster in the Arabidopsis root epidermal cells. It is possible the diagonal bias found in BY-2 cells is dependent on growth and nucleation during the drug treatment. This effect could be much smaller in the Arabidopsis root cells because of the shorter time of microtubule depolymerization.

Irrespective of whether the source of oriented nucleation in early array assembly is due to seeds from the previous array or another mechanism, our observations reveal the existence of a substantial class of noncanonical nucleations not associated with γ-TuRCs that contribute to the initiation of the cortical array. In simulation studies, we explored how these noncanonical nucleations may affect array reassembly and found this class of oriented nucleations to have the potential to significantly accelerate recovery of array density without significantly impeding the acquisition of the ultimate ordering that is driven by microtubule interactions. The existence of this mechanism may address a fundamental dilemma the plant cell faces in rebuilding an array from scratch. In interphase cells, nucleation from γ-TuRC complexes was observed to be approximately 10-fold more likely when they are localized to microtubules than to other locations at the cell cortex (Nakamura et al., 2010). If this reflects a fundamental property of γ-TuRC activation, then the cell may face limitations in how fast it can initiate new arrays when there are no existing cortical microtubules to recruit γ-TuRCs and contribute to their activation. Our live-cell observations and simulation studies reveal a class of nucleations that do not require γ-TuRC recruitment, and activation at cortical microtubules may act as a primer to accelerate the assembly of the new array.

MATERIALS AND METHODS

Plant Material

Tobacco (*Nicotiana tabacum*) BY-2 suspension cultured cells were grown according to standard protocols (Nagata et al., 1992). We stably transformed BY-2 cells using *Agrobacterium tumefaciens* LBA4404-mediated procedures with a reporter construct consisting of the enhanced synthetic GFP-TUA under control of the *Cauliflower mosaic virus* 35S promoter, kindly provided by Dr. S. Hasezawa (University of Tokyo, Japan; Kumagai et al., 2001). The BY-2 cell line expressing eGFP-FABD was generously provided by Dr. T. Ketelaar (Wageningen University; Ketelaar et al., 2004). We used *A. tumefaciens* to transform the pGCP2-GCP2-3xGFP construct, kindly provided by Masayoshi Nakamura and Takashi Hashimoto (Nara Institute of Science and Technology, Ikoma, Japan), into an Arabidopsis (*Arabidopsis thaliana*) Columbia-0-expressing 35s-mCherry-TUA5 (Gutierrez et al., 2009).

Specimen Mounting

Transformed cells were imaged in thin (approximately 10–20 μL) gas-permeable microchambers lined on one side with Biofoil (VivaScience) and a 24- × 24-mm coverslip on the other side as described earlier (Vos et al., 2004). Slides were sealed with 1:1:1 Vaseline:lanolin:paraffin. For oryzalin treatments, cells were immobilized in plastic flow cells (one channel of 100 μL with a height of 0.4 mm; Ibidi) that were pretreated with 1 mg/mL poly-L-Lys solution in deionized water for 30 min at room temperature. Ten flow cell volumes of 20 μM oryzalin (from 20 mM stock in DMSO) in BY-2 medium were perfused through the channel with cells and after 1 h washed out with constant perfusion of BY-2 medium at a flow rate greater than 0.1 mL/min. For latrunculin B and isoxaben experiments, 10 mL of a BY-2 culture was incubated for at least 3 h in 0.5 or 1.0 μM latrunculin B or at least 24 h in 10 μM isoxaben before adding 20 μM oryzalin and cell immobilization in a flow cell. Washes with latrunculin B or isoxaben were initiated after 1 h to allow the microtubule cytoskeleton to recover, but not the actin cytoskeleton or the cellulose microfibril production. The immobilization, the perfusion of medium with 0.1% (w/v) DMSO and 0.1% (w/v) ethanol, and the confocal imaging did not influence the cytoarchitecture or microtubule organization of the tobacco BY-2 cells (data not shown).

The Arabidopsis plants were grown on standard Hoagland medium and gently mounted between an objective slide and coverslip spaced by two strips of double-sided Scotch tape. For the oryzalin treatment, the plants were transferred to a six-well plate containing 1.0 μM oryzalin for an hour to depolymerize the microtubules. Oryzalin was washed out at a flow rate of approximately 0.5 mL deionized water min^{-1}.

Microscopy

For the long-term microtubule analysis, we used confocal laser scanning microscopy. Images and time-lapse movies were produced with a 63×/1.4-numerical aperture (NA) oil immersion differential interference contrast lens on an Axiovert 200M microscope equipped with a Pascal confocal laser scanning microscopy unit (Zeiss). The GFP was excited with the 488-nm argon laser and a 505-nm long-pass emission filter. To see all microtubules in the cortex, a pinhole of 1.5 to 2 airy disc units (1.0–1.4 μm in the *z* axis) was used. The scan time was 4 to 8 μs $pixel^{-1}$, and the temporal resolution was 3 to 5 min. Alternatively, time-lapse Z-series of 2.5-μm thickness were made on a Leica DM IRB microscope equipped with the perfect focusing system, a CSU22 spinning disk setup (Yokogawa), and a C9100 EM-CCD camera (Hamamatsu Photonics). We used a 100×/1.4-NA objective lens and excited the GFP with a 488-nm argon laser. Five 0.5-μm optical sections, each taking 250 ms, were typically obtained at 3-min intervals. The visible area with cortical microtubules varied from about 200 to 600 μm^2.

For the nucleation analysis, we used a confocal spinning disk microscope described earlier (Gutierrez et al., 2009), except that a Nikon Eclipse Ti microscope with the perfect focusing system and a 100× 1.45-NA oil objective replaced the Zeiss Axiovert 200. Alternatively, we used a total internal reflection fluorescence (TIRF) microscope on a Nikon Eclipse Ti microscope with

perfect focus system. We used a 100× 1.49-NA TIRF oil objective excited with a solid-state 478-nm laser (Cobolt) and using a Semrock 535/39 emission filter. The microscope was equipped with a manual Nikon TIRF arm and a QuantEM EM-CCD camera (Photometrics). We used 800-ms exposure time and a 2- or 2.14-s time interval for the spinning disk and TIRF microscope, respectively.

Data Analysis

Time-lapse images were converted into 8-bit TIFF file stacks with ImageJ (W.S. Rasband, National Institutes of Health, Bethesda, MD; http://rsb.info.nih.gov/ij/, 1997-2007). Z-stacks were converted to average or maximum projections of three to five sections. The ImageJ StackReg plug-in was used to align the images of a stack (Thévenaz et al., 1998). All visible microtubules in the images were traced using the semiautomatic ImageJ plug-in NeuronJ (version 1.01; Meijering et al., 2004). The microtubule tracings were stored as a series of x and y pixel coordinates with a maximum distance of five pixels in both the x and y direction between subsequent points. A Perl script was used to extract the line segments and distribute their lengths over 20 evenly spaced bins according to their angle with the x axis. The script corrects for the uneven distribution due to discrete pixel values of possible segment angles produced by NeuronJ (see Supplemental Materials and Methods S1 and Supplemental Fig. S6 for the verification procedure). As we could not distinguish between the plus and minus ends of microtubules, every line segment was assigned an angle in the interval from 0° to 180°. The bins had a width of 9° and were centered on 0°, 9°, etc., up to 171°.

For each image, the microtubule length density was obtained by dividing the total microtubule length by the area of the cortical section in the images. The angular distribution data are presented in contour plots produced with Origin (OriginLab) as the fraction of microtubule length at each time point. For clarity, an extra 180° bin is depicted as a copy of the 0° bin in each graph. The angle bins are along the y axis and time along the x axis, and a rainbow color gradient indicates the cumulative microtubule length or fraction in 20 equal-sized steps, ranging from blue (few microtubules) to red (maximum length or fraction). Plots of mean distributions of several experiments were produced by aligning the timing of individual cells to the moments of zero microtubules after breakdown or before repolymerization and averaging the fractions.

To calculate the increase in microtubule density after cytokinesis and oryzalin washout as well as the final plateau value, data from individual experiments were fitted with the linear function: If t > Tp, then density = P1 + P2 × Tp, else density = P1 + P2 × t, with Tp as the time to reach the plateau density. The time of emergence of diagonal (45° and 135°) and transverse (90°) microtubule ordering was analyzed by filtering the angle bins with two test functions: T for transverse ordering and D for diagonal ordering (see Supplemental Information and Supplemental Fig. S7). Both functions have the property that a randomized system yields a value of 0. A system that is perfectly ordered (in the transverse direction for T and the diagonal direction for D) produces a value of 1.

For the nucleation analysis, we determined the position in the cell, the time point, and the angle with respect to the cell axis, whether the nucleation was free or microtubule bound and the angle of the seed microtubule in case of branching nucleation. For further analysis, we only used the microtubule nucleations that were unbound. To assess whether a bias exists for nucleation along diagonal directions, we defined 15° degree bins around the 45°, 135°, 225°, and 315° directions and scored microtubules in these bins as being diagonal. We introduced a diagonal biasing parameter δ by equating the probability of a diagonal nucleation to a nondiagonal nucleation:

$$P_{\mathrm{diag}}(\delta) = \frac{\frac{1}{6}\delta}{\frac{1}{6}\delta + \frac{5}{6}(1-\delta)}$$

This parameter is normalized such that $\delta = 0$ implies there are no diagonal nucleations, $\delta = 1$ implies all nucleations are diagonal, while $\delta = 1/2$ is the neutral case in which there is no bias, in which case the proper unbiased weight 1/6 = 60°/360° is accorded to the diagonal bins. We then performed a maximum likelihood estimate of δ by evaluating the likelihood ratio:

$$\frac{L(\delta)}{L\left(\frac{1}{2}\right)} = \frac{P_{\mathrm{diag}}(\delta)^M \left(1 - P_{\mathrm{diag}}(\delta)\right)^{N-M}}{\left(\frac{1}{6}\right)^M + \left(\frac{5}{6}\right)^{N-M}}$$

where M is the number of diagonal microtubules observed out of a total of N. For the nucleations after cytokinesis, we have $M = 66$ and $n = 274$, yielding $\delta = 0.61$. For the nucleations after oryzalin washout, we have $M = 26$ and $n = 73$, yielding $\delta = 0.73$ (see Supplemental Fig. S8, A and B). Note that a standard one-tailed binomial analysis also rejects the null hypothesis of no bias with $P < 0.001$ for the postcytokinesis case and $P < 0.0001$ for the oryzalin washout case.

Simulation Methods

We performed simulations of interacting cortical microtubules using the event-based algorithm (Tindemans et al., 2010). The simulations are implemented on a cylindrical cell geometry with a length of 80 μm and a radius of 40 μm. Microtubules that impinge on the edges of the cylinder undergo catastrophes, a boundary condition that was shown to robustly select a transverse orientation of the steady-state array (Allard et al., 2010; Eren et al., 2010).

The kinetic parameters for the dynamics of the microtubule plus ends are based on Vos et al. (2004): growth speed = 0.08 μm s^{-1}, shrinkage speed = 0.16 μm s^{-1}, spontaneous catastrophe rate (switch from growing to shrinking state) = 0.003 s^{-1} (a value slightly lower than that of Vos et al. [2004], consistent with a likely overestimation of this quantity in that work due to undetected collision-induced catastrophes), and rescue rate (switch from shrinking to growing state) = 0.007 s^{-1}. The minus ends of microtubules shrink with a constant treadmilling speed of 0.01 μm s^{-1}, following Shaw et al. (2003) and identical to Deinum et al. (2011).

The results of angle-dependent collisions between growing microtubules and obstructing ones follow the simplified scheme also employed by Allard et al. (2010), Eren et al. (2010), and Deinum et al. (2011). All collisions with an incidence angle below 40° result in collision-induced bundling, where the incoming microtubule changes direction and continues to grow along the obstructing one. The outcomes of steep angle encounters vary greatly from cell type and stage (Wasteneys and Ambrose, 2009); therefore, we measured these outcomes in our 2-s data set after cytokinesis in BY-2 cells. We found that of 70 encounters greater than 40° in four cells, 14 (20%) encounters induced a catastrophe, and 56 (80%) resulted in a crossover. Therefore, in our simulations, collisions with an incidence angle larger than 40° have a 20% probability of undergoing an induced catastrophe, where they switch to a shrinking state, and an 80% probability of simply crossing over the obstructing microtubule.

New microtubules are nucleated at a constant overall rate of 0.0002 s^{-1} μm^{-2}, which we estimated from our observations of the nucleations after cytokinesis (Deinum et al., 2011). Nucleations occur either at an arbitrary location in the model cortex or from a microtubule. We modeled the portioning of nucleation events between microtubule-free and microtubule-bound by a density-dependent chemical equilibrium, which accounts for the affinity of nucleation complexes for the microtubules. The fraction of microtubule-bound nucleations is given by

$$f_{\mathrm{bound}} = \frac{\rho}{\rho + \rho_{\frac{1}{2}}}$$

where ρ is the (time-dependent) length density (μm μm^{-2}) of the microtubules, and the crossover density $\rho_{1/2} = 0.1$ μm μm^{-2} determines the location of the equilibrium, which we chose in order to match the observed timescale of the crossover toward the final transversely ordered state. The microtubule-bound nucleations have an orientational distribution with respect to the parent microtubule, which is a coarse-grained representation (Deinum et al., 2011) of the experimentally observed patterns (Chan et al., 2009). We reduced the rate of unbound nucleations by the a factor of 10 to 0.00002 s μm^{-2}, following the data presented by Nakamura et al. (2010) for a steady-state microtubule array.

At the start of the simulations, we add a finite pool of microtubule fragments with the density of 0.1 μm^{-2} and an activation rate of 0.003 s^{-1}. These values were based on the free nucleation rate of BY-2 cells after cytokinesis. Only these reactivating microtubule fragments have a bias toward the diagonal directions of 45° and 135°. This bias was implemented by drawing the direction of nucleation with respect to the parent microtubule from the following distribution

$$\psi(\theta) = \frac{1}{2\pi I_0(\alpha)} \exp\left\{\alpha \cos 4\left(\theta - \frac{\pi}{4}\right)\right\}$$

where the angle θ is expressed in radians, α is a parameter that sets the degree of bias, and I_0 is a modified Bessel function of the first kind (Abramowitz and Stegun, 1970). We chose $\alpha = 1.5$, which reproduces the experimentally determined ratio between the nucleations in 15° bins around the diagonal directions and those in the remaining directions, for the case after cytokinesis. In the control simulations, this pool of microtubule nucleations was not present.

All simulations were started from an initially empty cortex. The time evolution of the angular distributions of microtubules was analyzed using the same filters also used for the experiments (see Supplemental Materials and Methods S1). The microtubule density is reported in terms of an optical density in which overlapping microtubules in bundles do not separately

contribute to the density but only the bundle as a whole, mimicking the values measured in the experiments. All simulation results are the average of 500 independent simulations performed with the same parameters. The results were also used for subsequent calculations of D and T and Figure 5C.

Supplemental Data

The following materials are available in the online version of this article.

Supplemental Figure S1. Microtubule ordering after cell division in two daughter cells.

Supplemental Figure S2. Contour plot with the angular distribution of the microtubule length fractions over time of a BY-2 cell expressing 35s-GFP-TUA that progresses into prophase after oryzalin washout.

Supplemental Figure S3. Cortical microtubule density and angle distribution after oryzalin treatment in the presence of latrunculin B.

Supplemental Figure S4. Cortical microtubule density and angle distribution after oryzalin treatment in the presence of isoxaben.

Supplemental Figure S5. Angle frequency distribution histograms cortical microtubules in individual Arabidopsis root epidermal cells.

Supplemental Figure S6. Verification of the Perl script through two different line drawings.

Supplemental Figure S7. Depiction of the filter functions used to calculate the weighted ordering parameters, D and T, from the microtubule density angle fractions.

Supplemental Figure S8. Plot of the likelihood ratio for a biased versus an unbiased model of diagonal nucleations as a function of the bias parameter $\bar{o}$ on the basis of the data for cytokinesis.

Supplemental Movie S1. Movie of the cortex of a GFP-TUA expressing tobacco BY-2 cell imaged from late cytokinesis into interphase.

Supplemental Movie S2. Movie of the cortex of a GFP-TUA expressing tobacco BY-2 cells during oryzalin treatment.

Supplemental Movie S3. Microtubule nucleations after oryzalin washout in BY-2 cells expressing GFP-TUA.

Supplemental Movie S4. Cortical microtubule array during interphase in Arabidopsis root epidermal cells expressing GCP2-3xGFP and mCherry-TUA5, in which microtubule nucleations can be observed.

Supplemental Movie S5. Microtubule nucleations after oryzalin washout in Arabidopsis root epidermal cells expressing GCP2-3xGFP and mCherry-TUA5.

Supplemental Movie S6. Oryzalin wash in and wash out in Arabidopsis root epidermal cells expressing mCherry-TUA5.

Supplemental Movie S7. Oryzalin wash out in Arabidopsis root epidermal cells expressing mCherry-TUA5 in the presence of visible microtubule fragments.

Supplemental Materials and Methods S1.

ACKNOWLEDGMENTS

We thank Seiichiro Hasezawa (University of Tokyo) for the generous gift of the tobacco GFP-TUA construct and Tijs Ketelaar (Wageningen University) for the BY-2 cell line expressing the GFP-FABD. We thank Masayoshi Nakamura (Carnegie Institution for Science) and Takashi Hashimoto (Nara Institute of Science and Technology) for sharing the GCP2-3xGFP construct. We also thank Tijs Ketelaar for helpful discussions.

Received July 20, 2012; accepted January 4, 2013; published January 8, 2013.

LITERATURE CITED

Abramowitz M, Stegun IA (1970) Handbook of Mathematical Functions with Formulas, Graphs, and Mathematical Tables, Ed 9. U.S. Government Printing Office, Washington, DC

Allard JF, Wasteneys GO, Cytrynbaum EN (2010) Mechanisms of self-organization of cortical microtubules in plants revealed by computational simulations. Mol Biol Cell **21:** 278–286

Ambrose C, Allard JF, Cytrynbaum EN, Wasteneys GO (2011) A CLASP-modulated cell edge barrier mechanism drives cell-wide cortical microtubule organization in Arabidopsis. Nat Commun **2:** 430

Bartolini F, Gundersen GG (2006) Generation of noncentrosomal microtubule arrays. J Cell Sci **119:** 4155–4163

Baskin TI (2001) On the alignment of cellulose microfibrils by cortical microtubules: a review and a model. Protoplasma **215:** 150–171

Buschmann H, Lloyd CW (2008) Arabidopsis mutants and the network of microtubule-associated functions. Mol Plant **1:** 888–898

Chan J, Calder GM, Doonan JH, Lloyd CW (2003) EB1 reveals mobile microtubule nucleation sites in Arabidopsis. Nat Cell Biol **5:** 967–971

Chan J, Eder M, Crowell EF, Hampson J, Calder G, Lloyd C (2011) Microtubules and CESA tracks at the inner epidermal wall align independently of those on the outer wall of light-grown Arabidopsis hypocotyls. J Cell Sci **124:** 1088–1094

Clarke PR, Zhang C (2008) Spatial and temporal coordination of mitosis by Ran GTPase. Nat Rev Mol Cell Biol **9:** 464–477

Chan J, Sambade A, Calder G, Lloyd C (2009) *Arabidopsis* cortical microtubules are initiated along, as well as branching from, existing microtubules. Plant Cell **21:** 2298–2306

Crowell EF, Timpano H, Desprez T, Franssen-Verheijen T, Emons AM, Höfte H, Vernhettes S (2011) Differential regulation of cellulose orientation at the inner and outer face of epidermal cells in the *Arabidopsis* hypocotyl. Plant Cell **23:** 2592–2605

Deinum EE, Tindemans SH, Mulder BM (2011) Taking directions: the role of microtubule-bound nucleation in the self-organization of the plant cortical array. Phys Biol **8:** 056002

Dhonukshe P, Weits DA, Cruz-Ramirez A, Deinum EE, Tindemans SH, Kakar K, Prasad K, Mähönen AP, Ambrose C, Sasabe M, et al (2012) A PLETHORA-auxin transcription module controls cell division plane rotation through MAP65 and CLASP. Cell **149:** 383–396

Dixit R, Cyr R (2004) Encounters between dynamic cortical microtubules promote ordering of the cortical array through angle-dependent modifications of microtubule behavior. Plant Cell **16:** 3274–3284

Ehrhardt DW, Shaw SL (2006) Microtubule dynamics and organization in the plant cortical array. Annu Rev Plant Biol **57:** 859–875

Eren EC, Dixit R, Gautam N (2010) A three-dimensional computer simulation model reveals the mechanisms for self-organization of plant cortical microtubules into oblique arrays. Mol Biol Cell **21:** 2674–2684

Fujita M, Himmelspach R, Hocart CH, Williamson RE, Mansfield SD, Wasteneys GO (2011) Cortical microtubules optimize cell-wall crystallinity to drive unidirectional growth in Arabidopsis. Plant J **66:** 915–928

Green PB (1962) Mechanism for plant cellular morphogenesis. Science **138:** 1404–1405

Gruss OJ, Vernos I (2004) The mechanism of spindle assembly: functions of Ran and its target TPX2. J Cell Biol **166:** 949–955

Gutierrez R, Lindeboom JJ, Paredez AR, Emons AMC, Ehrhardt DW (2009) Arabidopsis cortical microtubules position cellulose synthase delivery to the plasma membrane and interact with cellulose synthase trafficking compartments. Nat Cell Biol **11:** 797–806

Hardham AR, Gunning BES (1978) Structure of cortical microtubule arrays in plant cells. J Cell Biol **77:** 14–34

Hawkins RJ, Tindemans SH, Mulder BM (2010) Model for the orientational ordering of the plant microtubule cortical array. Phys Rev E Stat Nonlin Soft Matter Phys **82:** 011911

Ketelaar T, Allwood EG, Anthony R, Voigt B, Menzel D, Hussey PJ (2004) The actin-interacting protein AIP1 is essential for actin organization and plant development. Curr Biol **14:** 145–149

Kirik A, Ehrhardt DW, Kirik V (2012) TONNEAU2/FASS regulates the geometry of microtubule nucleation and cortical array organization in interphase *Arabidopsis* cells. Plant Cell **24:** 1158–1170

Kumagai F, Yoneda A, Tomida T, Sano T, Nagata T, Hasezawa S (2001) Fate of nascent microtubules organized at the M/G1 interface, as visualized by synchronized tobacco BY-2 cells stably expressing GFP-tubulin: time-sequence observations of the reorganization of cortical microtubules in living plant cells. Plant Cell Physiol **42:** 723–732

Ledbetter MC, Porter KR (1963) A microtubule in plant cell fine structure. J Cell Biol **19:** 239–250

Lucas JR, Courtney S, Hassfurder M, Dhingra S, Bryant A, Shaw SL (2011) Microtubule-associated proteins MAP65-1 and MAP65-2 positively

regulate axial cell growth in etiolated *Arabidopsis* hypocotyls. Plant Cell **23:** 1889–1903

Meijering E, Jacob M, Sarria JCF, Steiner P, Hirling H, Unser M (2004) Design and validation of a tool for neurite tracing and analysis in fluorescence microscopy images. Cytometry A **58:** 167–176

Morejohn LC, Bureau TE, Molebajer J, Bajer AS, Fosket DE (1987) Oryzalin, a dinitroaniline herbicide, binds to plant tubulin and inhibits microtubule polymerization in vitro. Planta **172:** 252–264

Murata T, Sonobe S, Baskin TI, Hyodo S, Hasezawa S, Nagata T, Horio T, Hasebe M (2005) Microtubule-dependent microtubule nucleation based on recruitment of gamma-tubulin in higher plants. Nat Cell Biol **7:** 961–968

Nagata T, Nemoto Y, Hasezawa S (1992) Tobacco BY-2 cell line as the HeLa cell in the cell biology of higher plants. Int Rev Cytol **132:** 1–30

Nakamura M, Ehrhardt DW, Hashimoto T (2010) Microtubule and katanin-dependent dynamics of microtubule nucleation complexes in the acentrosomal Arabidopsis cortical array. Nat Cell Biol **12:** 1064–1070

Paredez AR, Somerville CR, Ehrhardt DW (2006) Visualization of cellulose synthase demonstrates functional association with microtubules. Science **312:** 1491–1495

Pastuglia M, Azimzadeh J, Goussot M, Camilleri C, Belcram K, Evrard JL, Schmit AC, Guerche P, Bouchez D (2006) γ-Tubulin is essential for microtubule organization and development in *Arabidopsis*. Plant Cell **18:** 1412–1425

Rogers GC, Rusan NM, Peifer M, Rogers SL (2008) A multicomponent assembly pathway contributes to the formation of acentrosomal microtubule arrays in interphase Drosophila cells. Mol Biol Cell **19:** 3163–3178

Rusan NM, Rogers GC (2009) Centrosome function: sometimes less is more. Traffic **10:** 472–481

Shaw SL, Kamyar R, Ehrhardt DW (2003) Sustained microtubule treadmilling in Arabidopsis cortical arrays. Science **300:** 1715–1718

Somerville C (2006) Cellulose synthesis in higher plants. Annu Rev Cell Dev Biol **22:** 53–78

Teixidó-Travesa N, Roig J, Lüders J (2012) The where, when and how of microtubule nucleation: one ring to rule them all. J Cell Sci **125:** 4445–4456

Thévenaz P, Ruttimann UE, Unser M (1998) A pyramid approach to subpixel registration based on intensity. IEEE Trans Image Process **7:** 27–41

Tindemans SH, Hawkins RJ, Mulder BM (2010) Survival of the aligned: ordering of the plant cortical microtubule array. Phys Rev Lett **104:** 058103

Vos JW, Dogterom M, Emons AMC (2004) Microtubules become more dynamic but not shorter during preprophase band formation: a possible "search-and-capture" mechanism for microtubule translocation. Cell Motil Cytoskeleton **57:** 246–258

Wasteneys GO (2002) Microtubule organization in the green kingdom: chaos or self-order? J Cell Sci **115:** 1345–1354

Wasteneys GO, Ambrose JC (2009) Spatial organization of plant cortical microtubules: close encounters of the 2D kind. Trends Cell Biol **19:** 62–71

Wasteneys GO, Williamson RE (1989a) Reassembly of microtubules in *Nitella tasmanica*: quantitative analysis of assembly and orientation. Eur J Cell Biol **50:** 76–83

Wasteneys GO, Williamson RE (1989b) Reassembly of microtubules in *Nitella tasmanica*: assembly of cortical microtubules in branching clusters and its relevance to steady-state microtubule assembly. J Cell Sci **93:** 705–714

Weerdenburg C, Seagull RW (1988) The effects of taxol and colchicine on microtubule and microfibril arrays in elongating plant cells in culture. Can J Bot **66:** 1707–1716

Whittington AT, Vugrek O, Wei KJ, Hasenbein NG, Sugimoto K, Rashbrooke MC, Wasteneys GO (2001) MOR1 is essential for organizing cortical microtubules in plants. Nature **411:** 610–613